



DIFFERENTIAL CROSS SECTION MEASUREMENTS OF FAST NEUTRON SCATTERING

FOR ^{208}Pb , ^{232}Th AND ^{238}U AT 2,5 MeV.

by

G. HAOUAT, J. SIGAUD, J. LACHKAR, Ch. LAGRANGE,

B. DUCHEMIN, Y. PATIN

Service de Physique Nucléaire
Centre d'Etudes de Bruyères-le-Châtel
B.P. n° 561
92542-MONTROUGE-CEDEX-FRANCE-

ABSTRACT -

The scattering of neutrons from ^{208}Pb , ^{232}Th and ^{238}U has been studied at 2.5 MeV incident energy. The measurements were carried out using the four-angle time-of-flight neutron spectrometer of the Centre d'Etudes de Bruyères-le-Châtel. The overall neutron energy resolution was about 30 keV and, therefore, neutrons scattered by the ground state and the first 2^+ and 4^+ excited states of ^{232}Th and ^{238}U were experimentally resolved. For the three isotopes, elastic differential cross sections were obtained over the angular range from 20 to 160 deg. For ^{232}Th and ^{238}U , differential cross sections for inelastic scattering to the first 2^+ state and the first 4^+ state were also obtained from 50 to 160 deg and from 40 to 150 deg respectively.

The data have been compared to calculations using a spherical optical potential for ^{208}Pb and a coupled-channel optical potential for the deformed ^{232}Th and ^{238}U nuclei, with a single set of potential parameters except for the $A^{1/3}$ radius dependence. The compound nucleus contribution was also taken into account. Values of the β_2 and β_4 deformation parameters have been derived from this study for ^{232}Th and ^{238}U . The experimental data for the three isotopes are fairly well reproduced by calculations.

I - INTRODUCTION -

Besides the applied interest in providing accurate neutron scattering data for actinides there is a basic interest in the study of these nuclei. It has been pointed out that, when the contributions of the strong collective states to the optical potential are taken into account explicitly by means of coupled-channel calculations, the strength and geometric parameters of the resulting potential may be valid over a broad mass range [1]. Thus, except for the deformation parameters, the optical potential parameters of a deformed nucleus would be expected to be essentially the same as those of a nearby spherical nucleus.

This procedure has been successfully used in the rare earth region for analyses of alpha-particle scattering [2], and of extensive neutron data on even-A isotopes of Nd and Sm [3,4]. These analyses of the neutron data indicated that, in addition to the usual $A^{1/3}$ radius dependence, the significant variables of the optical potential from one isotope to another were the isospin dependence and the potential deformation.

A similar analysis has been attempted, here, for nuclei with $A \geq 208$. A neutron scattering experiment [5] was undertaken for ^{208}Pb , ^{232}Th and ^{238}U , the first isotope being a spherical nucleus near in mass to these actinide nuclei. For each deformed nucleus, differential cross sections for elastic scattering and inelastic scattering to the lowest 2^+ and 4^+ states were measured at 2.5 MeV incident neutron energy over the angular range from 20 to 160 deg. In addition, the elastic differential cross sections for ^{208}Pb were concurrently measured. At the incident energy of 2.5 MeV, previous calculations predict that the direct interaction cross sections are maximum for inelastic scattering to the two first excited states of the deformed ^{232}Th and ^{238}U nuclei, and that, for both of them, the compound nucleus contribution is small for elastic as well as for inelastic scattering [6,7,8].

In the measurements presented here, the inelastic scattering to the lowest 2^+ and 4^+ states of ^{232}Th and ^{238}U (fig. 1) was experimentally resolved from the elastic scattering.

II - EXPERIMENTAL PROCEDURE AND DATA REDUCTION -

Differential cross sections measurements were carried out using the four detector neutron time-of-flight facility of the Centre d'Etudes de Bruyères-le-Châtel [9]. Characteristic details of the experimental set-up are given here.

1. Neutron production.

Incident neutrons of 2.50 MeV energy were produced from the ${}^7\text{Li}(p,n_0){}^7\text{Be}$ reaction. The super EN tandem Van de Graaff accelerator provided a proton beam of 4.18 MeV energy, pulsed at a repetition rate of 2.5 MHz and bunched into bursts with a time dispersion of 1 ns (FWHM). By using a post-pulsing system, burst widths as short as 0.7 ns were achieved, as checked by time-of-flight measurement of the prompt γ -rays from proton induced reactions in the target (fig. 2). The average current was typically 1.5 μA .

The target consisted of 99.8% pure ${}^7\text{Li}$ evaporated on a 2-cm-diameter by 1-mm-thick tantalum disc. The energy spread of the incident neutrons, due to lithium thickness, was about 10 keV. Lithium oxidization would cause a larger neutron energy spread. Therefore, during handling and transportation of the target from the evaporator to the beam vacuum system it was placed in an evacuated can and put, still under vacuum, on the target holder.

The energy difference between incident neutrons, from the ${}^7\text{Li}(p,n){}^7\text{Be}$ reaction which leave ${}^7\text{Be}$ in its ground state and in its first excited state (431 keV), was large enough to enable scattering measurements for the ground state of ${}^{208}\text{Pb}$, ${}^{232}\text{Th}$ and ${}^{238}\text{U}$ and for the two first excited states of ${}^{232}\text{Th}$ and ${}^{238}\text{U}$ (fig. 1).

2. Samples and neutron spectrometer.

The scattering geometry is illustrated in fig. 3. The 2.50 MeV neutrons were incident on cylindrical samples located at 0 deg with respect to the proton beam axis and 10.2 cm from the target. The ${}^{208}\text{Pb}$, ${}^{232}\text{Th}$ and ${}^{238}\text{U}$ samples were solid metal cylinders, having the same number of atoms (0.294 mole); they had a diameter of 1.5 cm and their height was 3.1, 3.4 and 2.1 cm for ${}^{208}\text{Pb}$, ${}^{232}\text{Th}$ and ${}^{238}\text{U}$ respectively. The ${}^{208}\text{Pb}$ was cast of metal isotopically separated to a purity of 86.5%, The thorium sample was cast of natural metal (i.e. ${}^{232}\text{Th}$). The uranium sample, with 99.7% of ${}^{238}\text{U}$ atoms, was machined from depleted uranium.

The scattered neutrons were detected by an array of four recoil proton detectors placed at 20 deg intervals. Each detector consisted of a 10-cm-diameter by 2.5-cm-thick NE 213 liquid scintillator optically coupled to an XP 1040 photomultiplier tube. Each detector was housed in a 1600-kg shield of lead and paraffin loaded with Li CO_3 and borax. Four 1-m-long shadow bars made of polyethylene and lead intercepted neutrons from the source in the detector direction. In order to avoid illumination of the shadow bar tips, a separate lead block was placed near the source. The size and position of this block depended on the location of the four-detector array. Intermediate 1.5- and 0.5-m-long collimators of paraffin, loaded with Li CO_3 and borax, were placed between the detector shielding and the shadow bars. They greatly reduced time independent background in the scattered neutron spectra ; moreover, the smaller collimators defined the acceptance solid angle of the detectors at the scatterer. The flight path from the sample to each detector was 8 m.

3. Data acquisition.

The block diagram of the electronic apparatus is shown in fig. 4. Data were collected using standard time-of-flight techniques. Neutron-gamma pulse shape discrimination was used to reject most of the γ -ray induced events in the scintillators ; this n- γ discrimination was of major importance for the runs with the ^{232}Th and ^{238}U samples. Fast pulses from the anode of the four photomultipliers were mixed, after being properly shaped by constant fraction discriminators. The time difference between the detector pulses and the delayed beam pick-off pulses, as measured by a time-to-amplitude converter (T.A.C.), determined the flight times of the scattered neutrons. The linear output of the T.A.C. was recorded in a two-parameter mode simultaneously with the linear output of the photomultipliers, which is proportional to the recoil proton energy. The identification of the detector, which provided the neutron pulse, was given by an auxiliary coincidence pulse. The nominal electronic resolution was 0.9 ns FWHM, as checked by coincidence measurement with a ^{22}Na γ -ray source. During the measurements, the dead time in counting electronics was found to be less than 0.5% and corrections for it were ignored.

Neutron scattering measurements for ^{208}Pb , ^{232}Th and ^{238}U were completed at 2.5 MeV energy over the angular range from 20 to 160 deg at 19 angles. Data were taken in running periods of 18 to 24 hours. At each angle, ^{208}Pb , ^{232}Th and ^{238}U samples were sequentially measured.

In the data reduction process, the time-of-flight spectra were extracted off-line for a neutron energy threshold of the detectors set at 0.5 MeV in order to reduce the time independent background.

Fig. 5 shows the time-of-flight spectra of the scattered neutrons from ^{232}Th and ^{238}U at 50 and 110 deg . These spectra show the high resolution obtained in the measurement. The full width at half maximum of the elastic groups is about 2.2 ns, corresponding to an energy resolution of 30 keV or so, for the neutron energy of 2.5 MeV. Thus, the elastic and inelastic neutron groups are easily resolved for ^{232}Th and ^{238}U .

4. Neutron flux monitoring.

The primary neutron flux was monitored by counting the 431 keV and 478 keV γ -rays, produced by proton induced reactions in ^7Li ; these two lines correspond to the transition from the first excited state to the ground state in ^7Be and ^7Li respectively. The γ -rays were detected by a time-of-flight gated Ge(Li) diode, set at 50 deg relative to the proton beam axis and placed at 6 m from the target. An auxiliary neutron detector, set at 55 deg relative to the proton beam axis, was used also as a monitor, in the time-of-flight mode.

The γ -ray and neutron monitoring systems were consistent with each other to within 1%, throughout the course of the measurements.

5. Detector efficiency.

The energy dependence of the detector efficiency was determined between 2.1 and 2.5 MeV relative to the efficiency at 2.5 MeV. We counted, at the incident proton energy of 4.18 MeV and at 0 deg with respect to the proton beam, neutron groups from the $^7\text{Li}(p,n)^7\text{Be}$ reaction which leave ^7Be in its ground and first excited states, and normalized to the known cross sections [10].

The absolute efficiency was not needed because we removed the sample and brought the detector to 0 deg and 8 m from the target in order to measure the incident neutron flux. Hence the incident and scattered fluxes were measured with the same detector.

6. Data reduction, corrections and uncertainties.

Sample-in and sample-out measurements were made. For each scattered neutron spectrum, background subtraction was achieved. Yields were obtained for isolated peaks in the spectra both by direct summation of counts and also by fitting gaussian forms to the peaks. For peaks too close to each other, yields were obtained by gaussian fitting procedures (fig. 5).

The yields were corrected for anisotropy effects in the incident neutron flux and finite size effects in the sample. The cross sections, prior to sample corrections, were determined with the following formula :

$$\frac{d\sigma}{d\Omega} (\theta_L, E_i) = \frac{N \cdot \epsilon}{N_0 \cdot n \cdot L \cdot \Omega_S} \quad (1)$$

where :

$\frac{d\sigma}{d\Omega} (\theta_L, E_i)$: is the differential cross section for the scattering of neutrons of incident energy E_i , at the laboratory angle θ_L ,

N, N_0 : are the monitor normalized yields for the scattering sample, at angle θ_L , and the incident flux at 0 deg respectively, as measured by the detector,

n : is the number of atoms per cm^3 in the sample,

L : is the average chord length of the sample, of radius R , in the incident neutron direction, assuming the disc approximation ($L = \frac{\pi}{2} R$),

Ω_S : is the solid angle of the sample at the target,

and ϵ : is the correction factor for the incident neutron flux anisotropy.

The cross sections given by this formula were then corrected for neutron flux attenuation in the sample, multiple scattering and geometrical effects, using the analytical method described by KINNEY [11], in order to give finally the scattering cross sections.

Normalization uncertainties assigned to the data were small since the incident and scattered neutron fluxes were measured with the same detector. Uncertainties in the measurements arose from counting statistics and background subtraction, monitor counting dispersion, detector efficiency and sample corrections. These contributions, listed in table 1, were added quadratically to give the experimental uncertainties.

III - RESULTS AND INTERPRETATION -

1. Results.

Differential cross section measurements for ^{208}Pb , ^{232}Th and ^{238}U were made at 2.5 MeV incident neutron energy. Elastic differential cross sections were determined between 20 and 160 deg for the three isotopes. Inelastic cross sections were obtained from 50 to 160 deg for the first 2^+ excited state in ^{232}Th (50 keV) and ^{238}U (45 keV), and from 40 to 150 deg for the first 4^+ excited state in ^{232}Th (162 keV) and ^{238}U (148 keV). The inelastic cross sections, at the forward angles, were not determined since it was difficult if not impossible to separate the inelastic peaks from the high yielded elastic peaks whose shape was distorted by multiple scattering effects.

The differential cross sections, corrected for finite size effects in the sample, are given, with their uncertainties, in table 2. The data and their uncertainties, as obtained prior to sample corrections, are quoted in table 3 ; these data may be useful for further analysis including sample corrections by Monte-Carlo methods.

The elastic scattering angular distribution for ^{208}Pb is displayed in fig. 6. The cross sections for elastic scattering and inelastic scattering to the first 2^+ and 4^+ excited states are plotted in fig. 7 for ^{232}Th and in fig. 8 for ^{238}U . The curves correspond to calculations that will be presented in Sec. III.2. For ^{238}U , the data of GUENTHER et al. [12] at 2.4 MeV and 115 deg, and of EGAN et al. [6] at 2.5 MeV and 90 deg are also plotted in fig. 8 ; the data of GUENTHER et al. [12] include only the inelastic scattering to the 2^+ and 4^+ states. Some recent measurements, also for ^{238}U , have been made over the angular range from 45 to 152 deg in 7 data points [13] ; they are in good overall agreement with the present data.

One notes, from figs. 7 and 8, the similarity between ^{232}Th and ^{238}U cross sections for the ground, 2^+ and 4^+ states ; this implies that these nuclei seem to have a similar behaviour with regards to neutron scattering. On the other hand, the elastic scattering angular distribution for ^{208}Pb (fig. 6) is smoother in shape than the actinide elastic distributions ; this suggests that the compound nucleus process is more important for ^{208}Pb than for ^{232}Th and ^{238}U at 2.5 MeV. Indeed, since the energy of the first excited state in ^{208}Pb is 2.614 MeV, only the elastic scattering is energetically possible at 2.5 MeV and, as a consequence, compound elastic scattering is believed to be important.

2. Interpretation.

The approach to the analysis of neutron scattering by the spherical ^{208}Pb and deformed ^{232}Th and ^{238}U isotopes has been to treat them as nuclei which are very similar except for changes in nuclear deformation. Thus, in this study, the same complex scattering potential was used for the three nuclei, except for the $A^{1/3}$ radius dependence, and the deformation parameters were considered as variables characteristic of each isotope. No isospin term was included in the scattering potential since the asymmetry parameter $\frac{N-Z}{A}$ has a small variation in going from ^{208}Pb to ^{238}U .

Cross section calculations take into account both the direct interaction and compound nucleus contributions to the scattering (see table 4). For the direct interaction calculations, the conventional spherical optical model was used for ^{208}Pb , and the coupled-channel optical model [14] for ^{232}Th and ^{238}U . The compound nucleus process was treated in the WOLFENSTEIN-HAUSER-FESHBACH formalism using generalized transmission coefficients. The compound nucleus calculations included as possible exit channels compound elastic scattering, inelastic scattering to discrete and continuum levels, radiative capture and fission.

Optical potential and deformation parameters for ^{238}U have been previously selected on the basis of low-energy neutron data, total cross sections and unresolved elastic and inelastic scattering data at high energies [8,15]. The same procedure was used here, mainly for ^{232}Th and ^{238}U , with special consideration of the present experimentally resolved scattering data ; this led to more accurate determination of the parameters with the same global consistency.

Values of the potential parameters which were determined are :

- Real potential : WOODS-SAXON shape

$$V_R = 46.2 (\pm 0.4) - 0.3 E \quad , \text{ MeV}$$

$$R_R = 1.26 A^{1/3} \quad , \text{ fm}$$

$$a_R = 0.63 \quad , \text{ fm}$$

- Imaginary potential : derivative WOODS-SAXON shape

$$W_D = 3.6 (\pm 0.3) + 0.4 E \quad , \text{ MeV}$$

$$R_D = 1.26 A^{1/3} \quad , \text{ fm}$$

$$a_D = 0.52 \quad , \text{ fm}$$

- Spin-orbit potential : THOMAS-FERMI shape

$$V_{SO} = 6.2 (\pm 0.3) \quad , \text{ MeV}$$

$$R_{SO} = 1.12 A^{1/3} \quad , \text{ fm}$$

$$a_{SO} = 0.47 \quad , \text{ fm.}$$

The symbols E and A represent the incident neutron energy, in MeV, and the atomic mass, in a.m.u., respectively. The radii are given with 1% accuracy, the diffusivenesses with 3%.

For the deformed nuclei, coupled-channel calculations were performed with a coupling basis 0^+ , 2^+ , 4^+ , assuming complex radial form factors ; for these calculations a modified version [16] of TAMURA'S code [17] JUPITOR-1 was used. The β_2 and β_4 deformation parameters were varied to fit the scattering data of ^{232}Th and ^{238}U .

It is shown in fig. 6 for ^{208}Pb , that the agreement between experimental and calculated elastic cross sections is very good for angles larger than 100 deg; however some minor differences remain between 45 and 90 deg , No improvement was obtained when the potential parameters of lead proposed by FU and PEREY were used [18]. The separated contributions for direct interaction and compound nucleus processes are shown in the same figure as dashed and dotted curves, respectively, It must be noted that, since only the elastic channel is open at 2.5 MeV, the compound nucleus contribution is comparable to or larger than the direct interaction one beyond 45 deg ; therefore, calculated angular distributions were relatively insensitive to variations in the imaginary potential depth. Since the data were taken with a high energy resolution, the

above-mentioned differences below 100 deg may result from effects of resonances, observed in the total cross section near 2.5 MeV by FOSTER and GLASGOW [19], which were not taken into account in the present calculations.

For ^{232}Th and ^{238}U , the calculations were started [5] with MOLLER's parameters [20], which for ^{232}Th are $\beta_2 = 0.206$, $\beta_4 = 0.086$ and for ^{238}U $\beta_2 = 0.216$, $\beta_4 = 0.067$. The calculated curves for the scattering to the ground state and to the first 2^+ excited state deviated from the observed ^{232}Th and ^{238}U distributions, mainly at large scattering angles ; this effect became more pronounced as one goes from ^{232}Th to ^{238}U . Moreover, the calculated cross sections for the second excited state were, for both nuclei, larger than the data by almost a factor of 2. The same enhancement was obtained by using the potential and deformation parameters of ^{238}U proposed by PRINCE [21].

The β_2 and β_4 deformation parameters of ^{232}Th and ^{238}U were, then, varied toward lower values. As shown in figs. 7 and 8a, a good agreement between calculations and data was obtained for the following values of the deformation parameters :

	for ^{232}Th	$\beta_2 = 0.190$	$\beta_4 = 0.071$
and	for ^{238}U	$\beta_2 = 0.198$	$\beta_4 = 0.057$

These values are given with an estimated accuracy of 5%. For ^{238}U , a much better agreement with these data is obtained by using the present set of parameters than that proposed in earlier studies [8,15] (fig. 8b) ; thus, evidence is shown that neutron elastic and inelastic scattering data give strong constraints to accurate determination of the potential and deformation parameters.

It should be noted that, for each of these nuclei, the β_2 value deduced from the present work is substantially lower than the recently determined β_2 values for the charge distribution [22,23], an effect which has already been observed in the rare earth region [3,4] ; for the β_4 values, such a comparison is not valid since the recently published values for this parameter differ by almost a factor of 5 [22,23].

SUMMARY -

Differential cross sections for neutron scattering by ^{208}Pb , ^{232}Th and ^{238}U have been measured at 2.5 MeV with an energy resolution of about 30 keV. Angular distributions were obtained for elastic scattering by the three isotopes and for inelastic scattering corresponding to the first 2^+ and 4^+ excited states of ^{232}Th and ^{238}U . They have been compared to calculations including direct interaction and compound nucleus contributions to the scattering. In these calculations, a spherical optical potential was used for ^{208}Pb and a deformed optical potential for the actinides. From the analysis presented here, it seems that a single set of potential parameters provides a fairly good description of neutron scattering by the spherical nucleus ^{208}Pb and the deformed nuclei ^{232}Th and ^{238}U . For these two last nuclei, values of the β_2 and β_4 deformation parameters were obtained by analysing together elastic and inelastic scattering data.

Extensive neutron scattering measurements, in progress in our laboratory at higher energy, are expected to provide more accurate potential parameters and precise values of β_2 and β_4 for ^{232}Th , ^{238}U and other nuclei in the same mass region.

ACKNOWLEDGMENTS -

We are indebted to Pr. A. MICHAUDON for his helpful advice and stimulating encouragement in the preparation of this work. We also wish to thank A. DANDINE who designed and operated the post-pulsing system which enabled us to perform such high resolution measurements.

REFERENCES

- [1] - N.K. GLENDENNING, D.L. HENDRIE and O.N. JARVIS, *Phys. Lett.* 26B (1968) 131.
- [2] - D.L. HENDRIE, N.K. GLENDENNING, B.G. HARVEY, O.N. JARVIS, H.H. DUHM, J. MAHONEY and J. SAUDINOS, *Phys. Lett.* 26B (1968) 127.
- [3] - R. SHAMU, G. HAOUAT, J. LACHKAR, Ch. LAGRANGE, M.T. McELLISTREM, Y. PATIN, J. SIGAUD, F. COÇU, E. BERNSTEIN and J. RAMIREZ, *Proc. Nat. Soviet Conf. on Neutron Physics, KIEV - Neitroniya Physica VOL.4* (1976) 237.
- M.T. McELLISTREM, J. LACHKAR, G. HAOUAT, Ch. LAGRANGE, Y. PATIN, R. SHAMU, J. SIGAUD and F. COÇU, *Proc. of the Conf. on Nuclear Cross Sections and Techn.*, WASHINGTON D.C. - NBS SP425 Vol. 2 (1975) 942.
- M.T. McELLISTREM et al. (to be published in *Phys. Rev.*).
- [4] - G. HAOUAT, J. LACHKAR, Ch. LAGRANGE, M.T. McELLISTREM, Y. PATIN, R. SHAMU and J. SIGAUD, *Bull. Am. Phys. Soc.* 20 (1975) 1196.
- R. SHAMU, G. HAOUAT, J. LACHKAR, M.T. McELLISTREM, Ch. LAGRANGE, J. DELAROCHE Y. PATIN and F. COÇU, *Proc. of the Intern. Conf. on the Interactions of Neutrons with nuclei, LOWELL, CONF 760715 P2* (1976) 1327.
- [5] - G. HAOUAT, J. SIGAUD, J. LACHKAR, Ch. LAGRANGE, B. DUCHEMIN and Y. PATIN, *Proc. of the Intern. Conf. on the Interactions of Neutrons with nuclei, LOWELL, CONF 760715 P2* (1976) 1330.
- [6] - J.J. EGAN, G.H. KEGEL, G.P. COUCHELL, A. MITTLER, B.K. BARNES, W.A. SCHIER, D.J. PULLEN, P. HARIHAR, T.V. MARCELLA, V.B. SULLIVAN, E. SHELDON and A. PRINCE, *Proc. Conf. on Nuclear Cross Sections and Technology, WASHINGTON, D.C. NBS SP425 Vol II* (1975) 950.
- [7] - P. GUENTHER and A.B. SMITH, *Proc. Conf. on Nuclear Cross Sections and Techn.*, WASHINGTON, D.C. NBS SP425 Vol II (1975) 862.
- [8] - Ch. LAGRANGE, *NEANDC Report JAERI - M - 5984* (1975) 58.
- [9] - J. LACHKAR, M.T. McELLISTREM, G. HAOUAT, Y. PATIN, J. SIGAUD and F. COÇU, *Phys. Rev.* C14 (1976) 933.

- [10] - H. LISKEIN and A. PAULSEN, *Atomic Data and Nuclear Data Tables* 15 (1975) 57.
- [11] - W.E. KINNEY, *Nucl. Inst. Meth.* 83 (1970) 15.
- [12] - P. GUENTHER, D. HAVEL and A. SMITH, *Argonne Nat. Lab. Report ANL/NDM* 16 (1975).
- [13] - G.H. KEGEL, *private communication*.
- [14] - T. TAMURA, *Revs. Mod. Phys.* 37 (1965) 679.
- [15] - J. JARY, Ch. LAGRANGE and P. THOMET, *INDC (FR) 9/L, NEANDC (E) 174 "L"*, (1976).
- [16] - Ch. LAGRANGE, (*unpublished*).
- [17] - T. TAMURA, *ORNL - 4152* (1967).
- [18] - G. Y. FU and F. G. PEREY, *ORNL - 4765* (1972).
- [19] - D.J. FOSTER and D.W. GLASGOW, *Phys. Rev.* C3 (1971) 576.
- [20] - P. MÖLLER, *Nucl. Phys.* A192 (1972) 529.
- [21] - A. PRINCE, *Nuclear Data for Reactors Vol II (I.A.E.A. VIENNA, 1970)* p. 825.
- [22] - J.P. DAVIDSON, D.A. CLOSE and J.J. MALINAFY, *Phys. Rev. Lett.* 32 (1974) 337.
- [23] - T. COOPER, W. BERTOZZI, J. HEISENBERG et al., *Phys. Rev.* C13 (1976) 1083.

TABLE I

Uncertainty estimates for cross section measurements

- Counting statistics in the peak and background subtraction	1 - 25%
- Dispersion of monitor indications	≤ 1%
- Detector efficiency	1 - 2%
- Sample corrections	1 - 3%

TABLE II : Differential cross sections for 2.5 MeV neutron scattering from ^{208}Pb , ^{232}Th and ^{238}U , after sample corrections have been performed. Sample correction procedure is described in the text. Cross sections are given in mb/sr.

θ_{CM} (deg)	^{208}Pb	^{232}Th			^{238}U		
	0^+ (ground state)	0^+ (ground state)	2^+ (50 keV)	4^+ (162 keV)	0^+ (ground state)	2^+ (45 keV)	4^+ (148 keV)
20.1	2616.4 ± 78.5	2697.1 ± 80.9			2768.8 ± 83.1		
30.1	1504.9 ± 76.7	1443.7 ± 43.3			1402.6 ± 42.1		
35.1	1058.1 ± 31.7	787.4 ± 31.5			762.0 ± 30.5		
40.2	683.4 ± 23.2	434.6 ± 21.7		13.6 ± 2.2	403.0 ± 20.1		15.6 ± 3.9
50.2	384.1 ± 20.7	56.5 ± 3.1	59.3 ± 5.9	17.0 ± 3.7	52.7 ± 2.7	40.1 ± 4.4	8.6 ± 1.7
55.2	303.8 ± 17.0	7.5 ± 0.5	51.9 ± 4.8	16.2 ± 2.5	6.7 ± 0.4	37.5 ± 4.1	10.2 ± 2.1
60.2	237.1 ± 11.9	9.0 ± 0.7	46.8 ± 4.7	18.0 ± 2.7	16.7 ± 0.9	40.8 ± 4.3	12.4 ± 2.2
70.2	193.4 ± 10.4	85.4 ± 5.3	49.1 ± 5.2	16.8 ± 2.5	108.1 ± 5.9	55.7 ± 6.6	12.1 ± 1.8
75.2	177.4 ± 8.0	110.5 ± 5.2	44.0 ± 4.8	15.3 ± 2.4	121.1 ± 6.6	53.7 ± 5.8	11.0 ± 2.5
80.2	170.6 ± 7.5	130.7 ± 6.5	48.0 ± 4.8	15.5 ± 2.6	156.3 ± 7.3	52.4 ± 5.0	10.7 ± 1.6
90.2	218.4 ± 11.4	136.7 ± 8.6	40.9 ± 3.1	16.6 ± 2.5	122.8 ± 5.2	47.0 ± 3.3	10.4 ± 1.0
95.2	252.7 ± 14.4	103.2 ± 8.3	25.8 ± 3.1	14.1 ± 1.8	100.9 ± 4.9	36.0 ± 3.6	12.1 ± 2.2
100.2	323.4 ± 14.2	94.0 ± 5.6	30.0 ± 3.3	13.2 ± 2.0	80.4 ± 4.4	29.0 ± 2.9	10.4 ± 1.5
110.2	315.3 ± 15.8	52.3 ± 2.6	23.5 ± 2.4	7.3 ± 1.2	33.9 ± 1.8	20.4 ± 1.9	10.1 ± 1.5
120.2	281.0 ± 11.8	18.7 ± 0.5	26.5 ± 2.8	5.7 ± 0.9	9.8 ± 0.8	23.0 ± 3.5	6.9 ± 1.4
130.2	234.6 ± 10.8	3.5 ± 0.6	30.3 ± 3.1	4.3 ± 0.8	2.9 ± 0.5	40.2 ± 4.1	5.0 ± 1.2
140.2	210.6 ± 7.8	8.4 ± 1.1	34.8 ± 3.5	3.1 ± 0.8	5.5 ± 0.6	36.2 ± 3.6	3.4 ± 1.0
150.1	287.5 ± 12.9	28.6 ± 1.7	31.8 ± 3.1	3.3 ± 0.9	25.4 ± 1.3	31.7 ± 2.9	2.3 ± 0.8
160.1	552.2 ± 23.7	65.6 ± 3.5	32.8 ± 3.0		56.7 ± 2.8	31.9 ± 3.3	

TABLE III : Differential cross sections for 2.5 MeV neutron scattering from ^{208}Pb , ^{232}Th and ^{238}U , prior to sample corrections, Cross sections are given in mb/sr.

θ_L (deg)	^{208}Pb	^{232}Th			^{238}U		
	0^+ (ground state)	0^+ (ground state)	2^+ (50 keV)	4^+ (162 keV)	0^+ (ground state)	2^+ (45 keV)	4^+ (148 keV)
20	2069.0 ± 57.9	2042.0 ± 52.2			1830.0 ± 51.2		
30	1234.4 ± 61.7	1118.3 ± 31.3			962.0 ± 28.9		
35	892.4 ± 25.0	629.0 ± 24.5			547.6 ± 20.3		
40	601.0 ± 19.2	361.7 ± 17.4		11.8 ± 1.9	309.5 ± 14.5		11.9 ± 3.0
50	357.1 ± 18.6	66.3 ± 3.5	52.4 ± 5.2	14.4 ± 3.2	65.3 ± 3.0	34.5 ± 3.9	7.1 ± 1.4
55	288.8 ± 15.6	23.0 ± 1.4	46.0 ± 4.2	13.8 ± 2.1	26.0 ± 1.2	31.6 ± 3.5	8.0 ± 1.7
60	232.6 ± 11.2	19.6 ± 1.5	41.4 ± 4.1	15.1 ± 2.3	26.7 ± 1.2	32.8 ± 3.4	9.3 ± 1.7
70	193.8 ± 9.9	72.6 ± 4.2	42.3 ± 4.4	14.2 ± 2.1	78.9 ± 3.7	41.5 ± 4.9	9.0 ± 1.4
75	180.2 ± 7.2	91.0 ± 4.1	38.2 ± 4.2	13.0 ± 2.1	87.2 ± 4.2	40.2 ± 4.3	8.3 ± 1.9
80	174.0 ± 6.6	106.4 ± 5.1	41.0 ± 4.1	13.1 ± 2.2	110.0 ± 4.8	39.4 ± 3.7	8.1 ± 1.2
90	209.5 ± 10.5	111.7 ± 6.8	35.5 ± 2.7	13.9 ± 2.1	89.8 ± 3.5	36.0 ± 2.5	7.9 ± 0.8
95	235.7 ± 13.2	86.5 ± 6.7	23.9 ± 2.9	11.9 ± 1.5	75.6 ± 3.5	28.8 ± 2.9	9.0 ± 1.6
100	290.0 ± 12.2	79.4 ± 4.6	27.0 ± 3.0	11.2 ± 1.7	61.9 ± 3.1	24.0 ± 2.4	7.9 ± 1.1
110	285.7 ± 13.7	46.6 ± 2.2	21.6 ± 2.2	6.6 ± 1.1	29.6 ± 1.5	17.8 ± 1.6	7.6 ± 1.1
120	261.7 ± 10.5	19.3 ± 1.5	23.5 ± 2.5	5.2 ± 0.8	11.5 ± 8.8	19.0 ± 2.9	5.5 ± 1.1
130	228.7 ± 10.1	6.2 ± 1.1	26.3 ± 2.7	4.0 ± 0.8	5.5 ± 1.0	30.0 ± 3.0	4.0 ± 1.0
140	212.5 ± 7.4	9.2 ± 1.4	29.8 ± 3.0	3.0 ± 0.8	6.8 ± 0.7	27.7 ± 2.8	2.9 ± 0.9
150	271.4 ± 11.7	24.3 ± 1.4	27.8 ± 2.7	3.1 ± 0.8	20.4 ± 1.0	25.0 ± 2.3	2.1 ± 0.7
160	470.0 ± 19.3	52.0 ± 2.6	28.7 ± 2.6		41.6 ± 1.9	25.4 ± 2.6	

TABLE IV

Direct interaction (DI) and compound nucleus (CN) contributions to the scattering integrated cross sections at 2.5 MeV neutron energy for ^{208}Pb , ^{232}Th and ^{238}U . The cross sections, given in mb, are calculated from the potential and deformation parameters presented in the text.

		DI	CN
^{208}Pb	0^+ (ground state)	4 445	2 582
^{232}Th	0^+ (ground state)	3 753	19
	2^+ (50 keV)	358	63
	4^+ (162 keV)	117	50
^{238}U	0^+ (ground state)	3 763	12
	2^+ (45 keV)	421	40
	4^+ (148 keV)	124	33

FIGURE CAPTIONS

- FIGURE 1 : Low-lying level schemes of ^{208}Pb , ^{232}Th and ^{238}U . For ^{232}Th and ^{238}U only the first four levels of the ground state rotational band are given. Excitation energies are given in MeV.
- FIGURE 2 : Time spectrum of the prompt γ -rays emitted by the ^7Li target and showing the proton burst shape. The full width at half maximum (FWHM) is 0.7 ns and the full width at one tenth of the maximum (FWTM) is 1.4 ns.
- FIGURE 3 : Experimental arrangement used to measure the differential cross sections of ^{208}Pb , ^{232}Th and ^{238}U at 2.5 MeV incident neutron energy.
- FIGURE 4 : Block diagram of the electronics used in the neutron time-of-flight spectrometer. The abbreviations are the following :
- ADC : analog-to-digital converter.
 - Amp : linear amplifier.
 - Beam P O : beam time pick-off.
 - Delay Amp : delay amplifier.
 - Delay Gen : gate and delay generator.
 - Det : neutron detector.
 - CFD : constant fraction discriminator.
 - Disc : fast discriminator.
 - Fast Mix : fast mixer.
 - Ident Sign: signal identification unit.
 - PSP : pulse shape discriminator.
 - SCA : single channel analyser.
 - Sum Amp : linear sum amplifier.
 - TAC : time-to-amplitude converter.
- FIGURE 5 : Time-of-flight spectra of 2.5 MeV neutrons scattered at 50 deg(a) and 110 deg (b) by ^{232}Th (above) and ^{238}U (below). The flight path is 8 m. The detector time resolution is ~ 2.2 ns, corresponding to an energy resolution of ~ 30 keV. The solid curves are fits to the peaks by gaussian shapes.

FIGURE 6 : Differential elastic neutron scattering cross sections at 2.5 MeV incident energy for ^{208}Pb . The upper solid curve is the sum of the compound nucleus (CN) plus direct interaction (DI) theoretical calculations. Separated contributions are shown as dashed (DI) and dotted (CN) curves.

FIGURE 7 : Neutron scattering cross sections at 2.5 MeV for elastic (0^+), first excited (2^+ , 50 keV) and second excited (4^+ , 162 keV) states in ^{232}Th . The solid curves are results of theoretical calculations as described in the text, Deformation parameters are given in the figure.

FIGURE 8 *a* : Neutron scattering cross sections at 2.5 MeV for elastic (0^+), first excited (2^+ , 45 keV) and second excited (4^+ , 148 keV) states in ^{238}U (squares). Also shown for comparison are the data of EGAN et al. [6] at the same energy (stars) and those of GUENTHER et al. [12] at 2.4 MeV (crosses). Solid curves are results of theoretical calculations. Deformation parameters are given in the figure.

b : Same experimental cross sections as in fig. 8a. Solid curves are results of calculations using potential and deformation parameters of references 8 and 15.

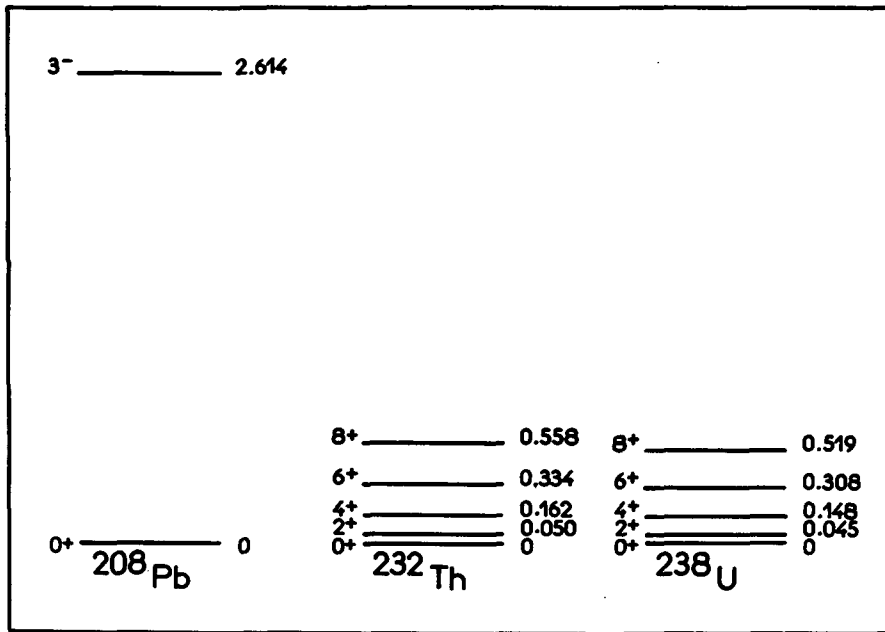


FIGURE 1

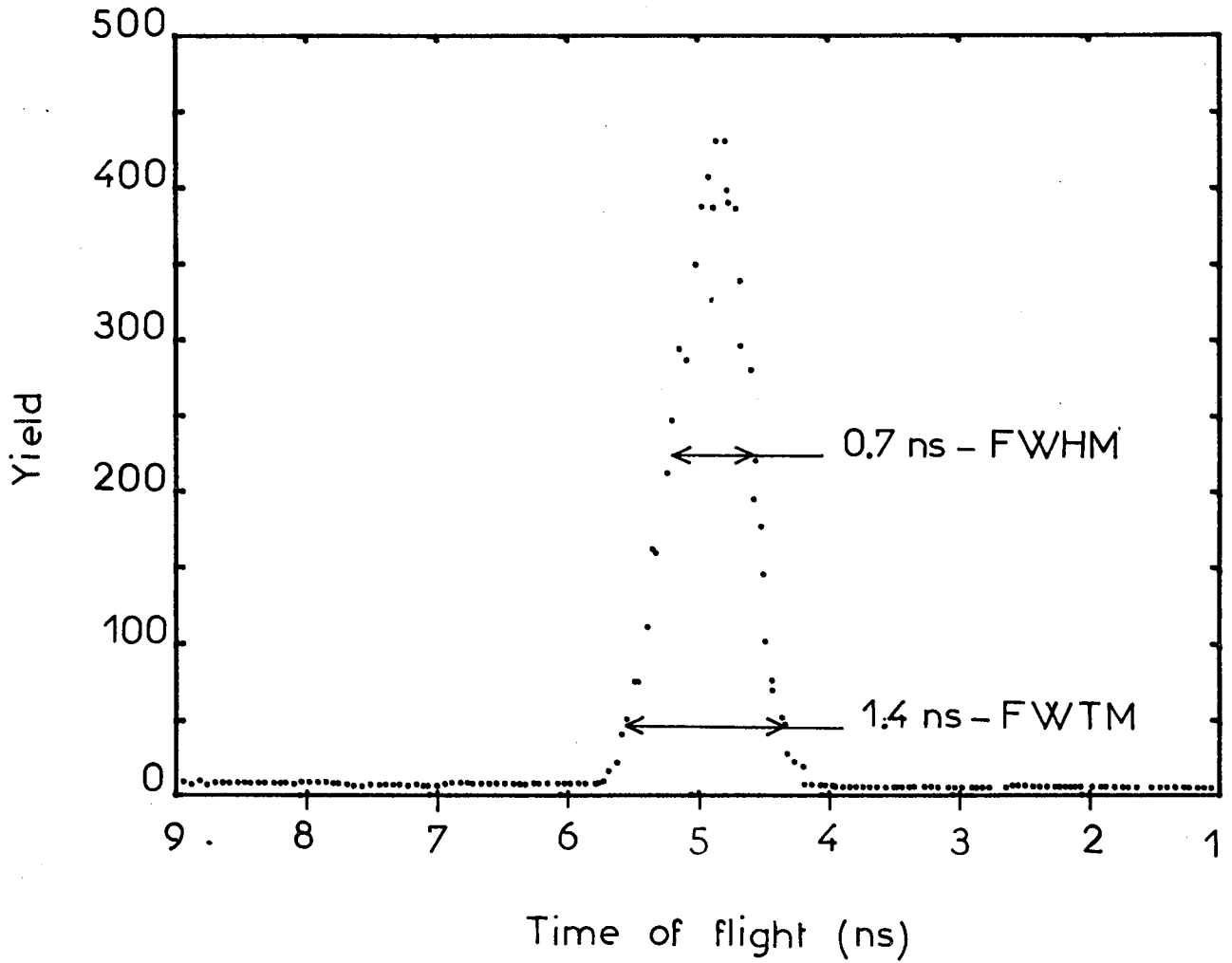


FIGURE 2

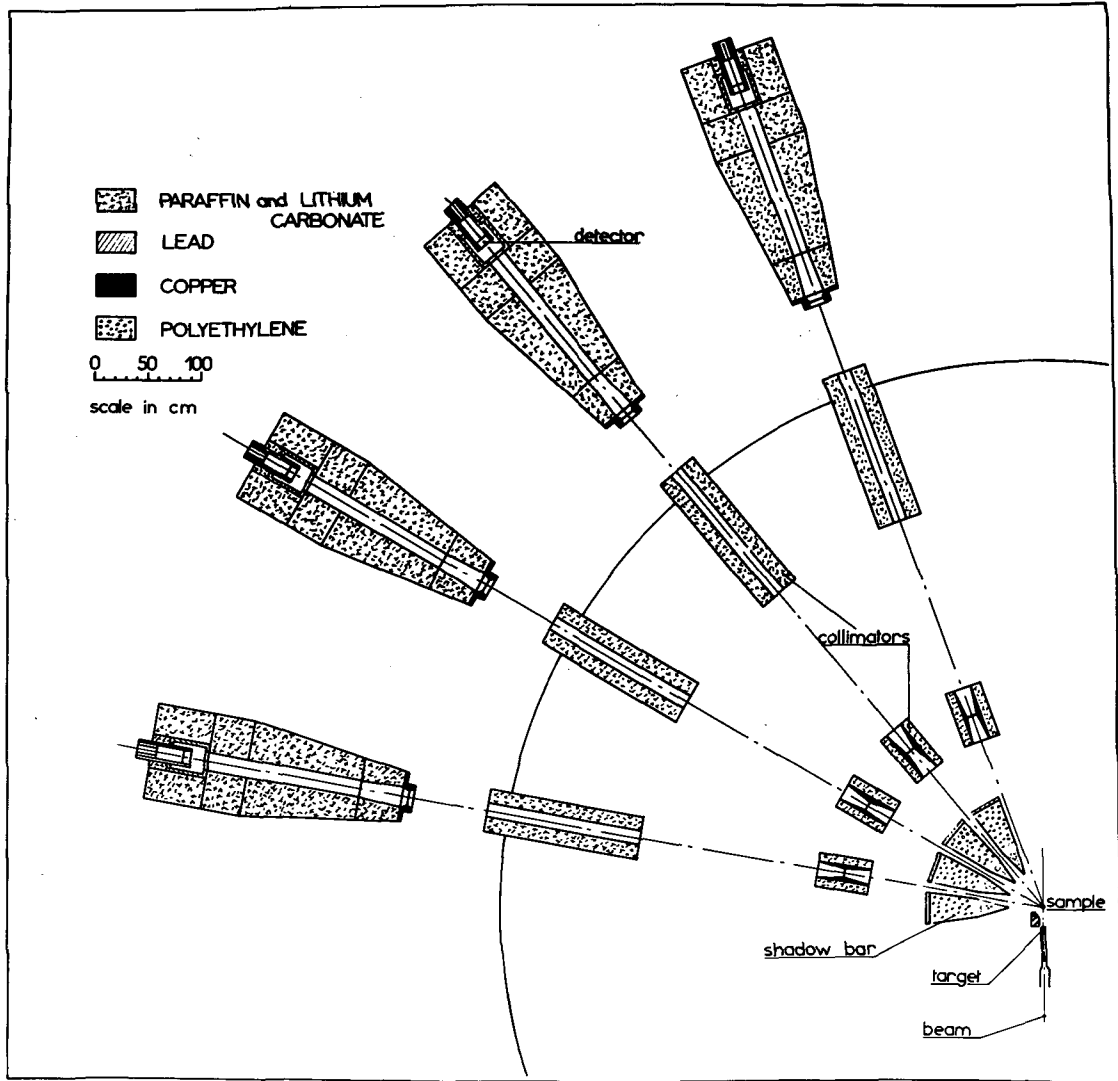


FIGURE 3

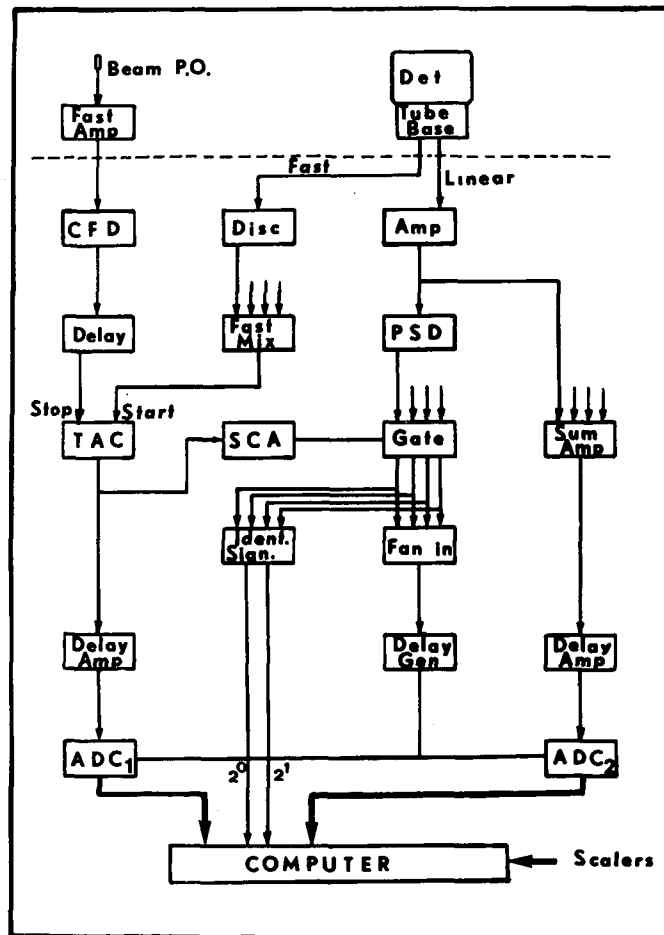


FIGURE 4

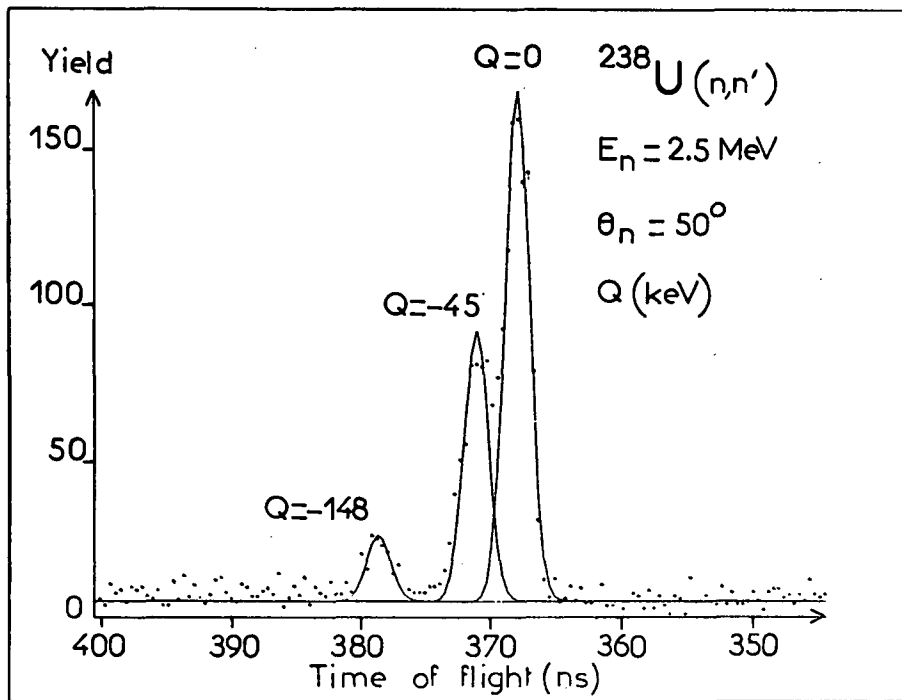
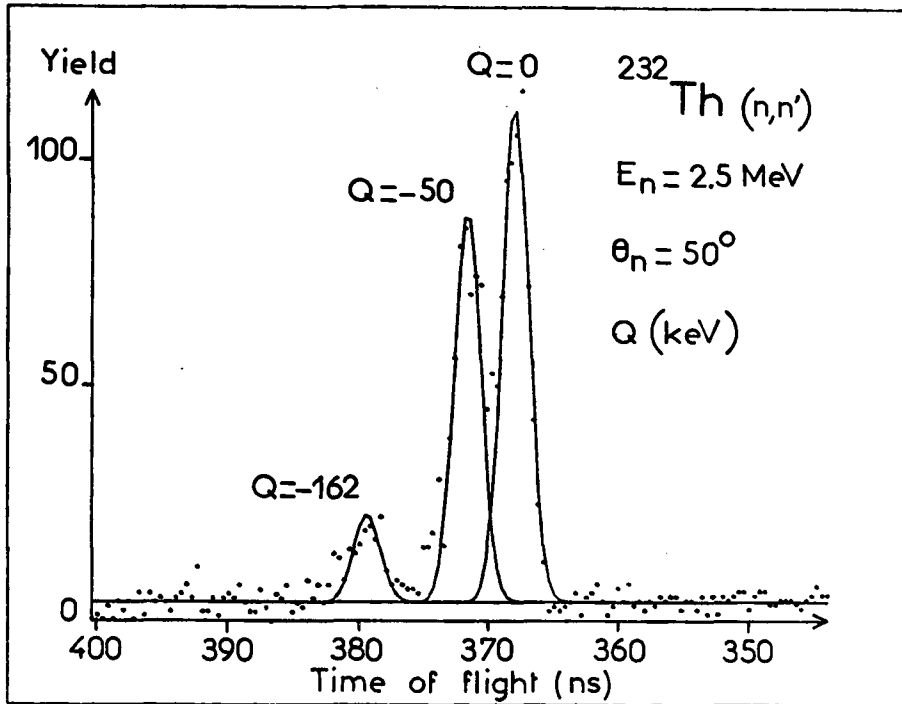


FIGURE 5a

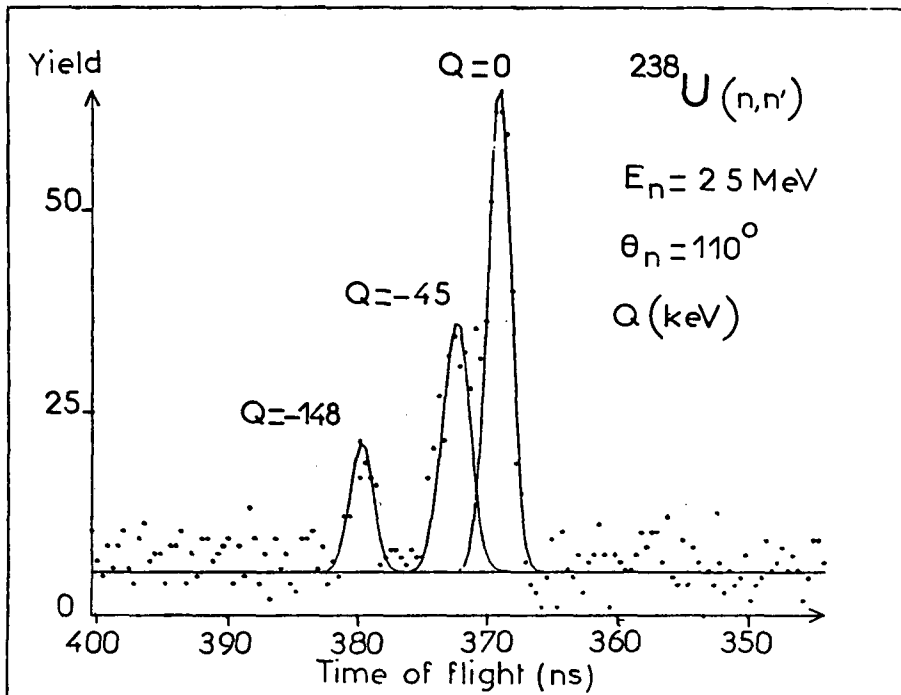
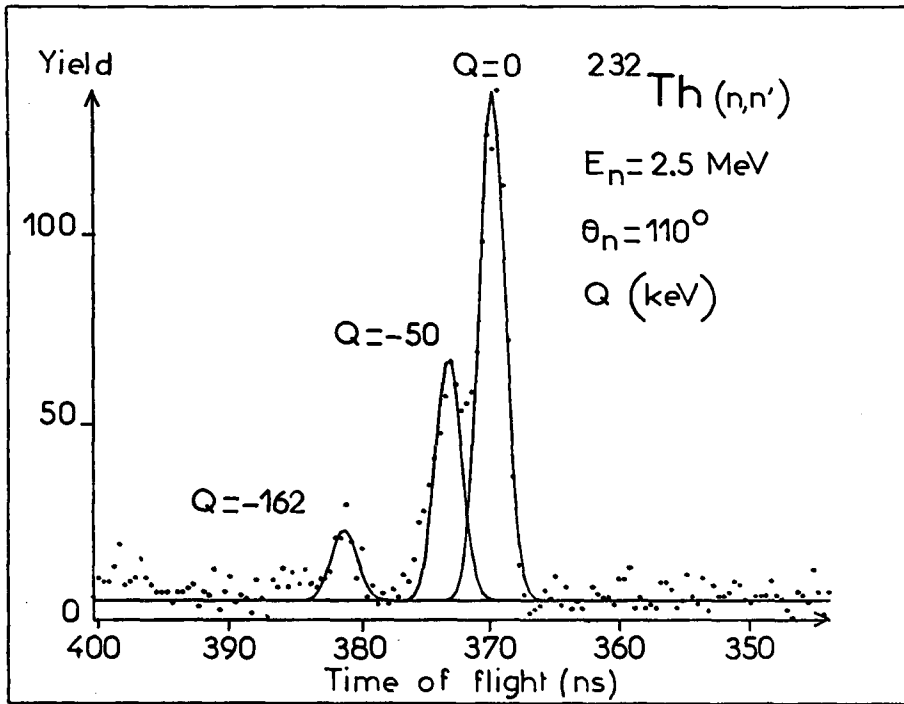


FIGURE 5b

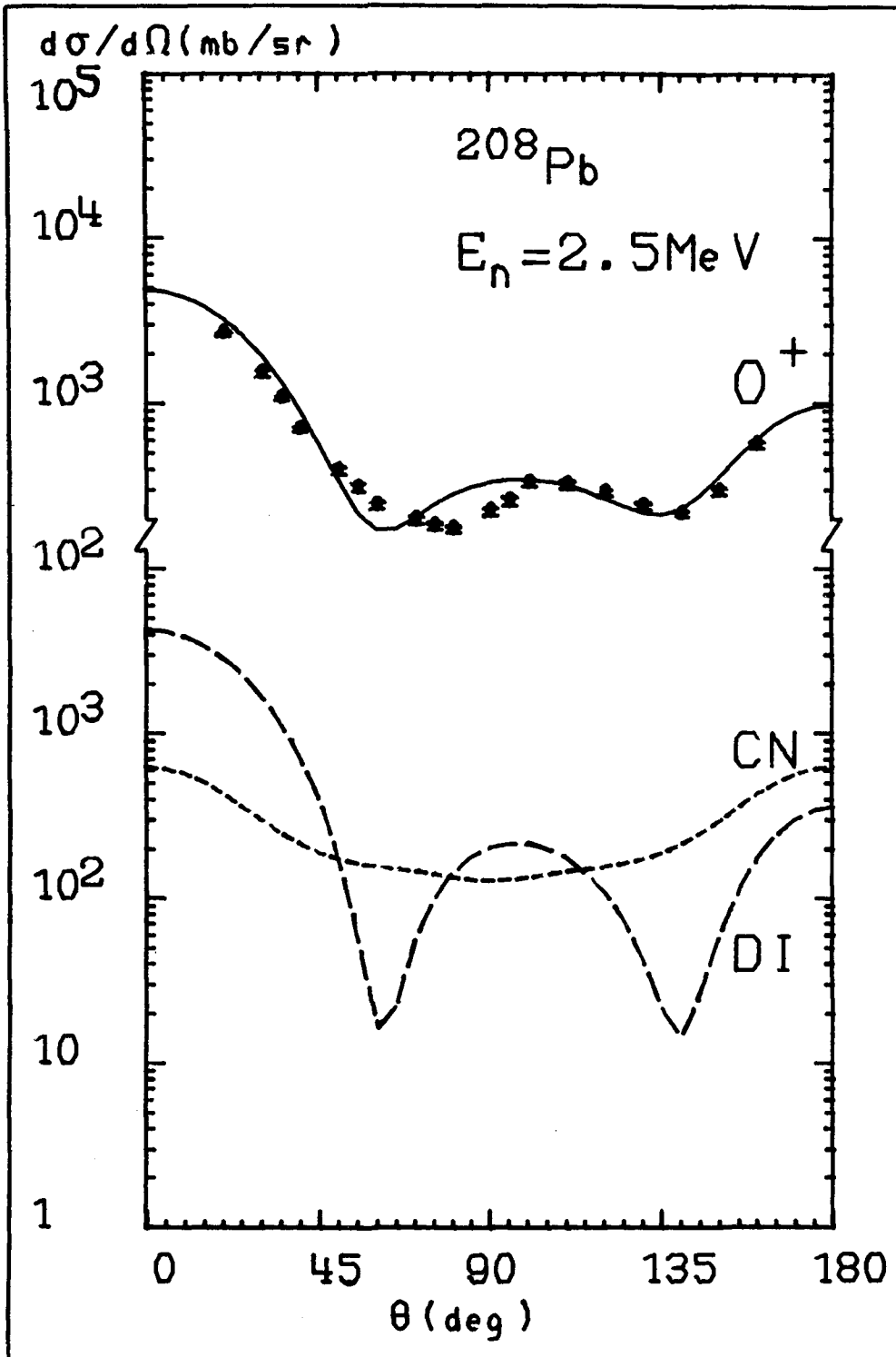


FIGURE 6

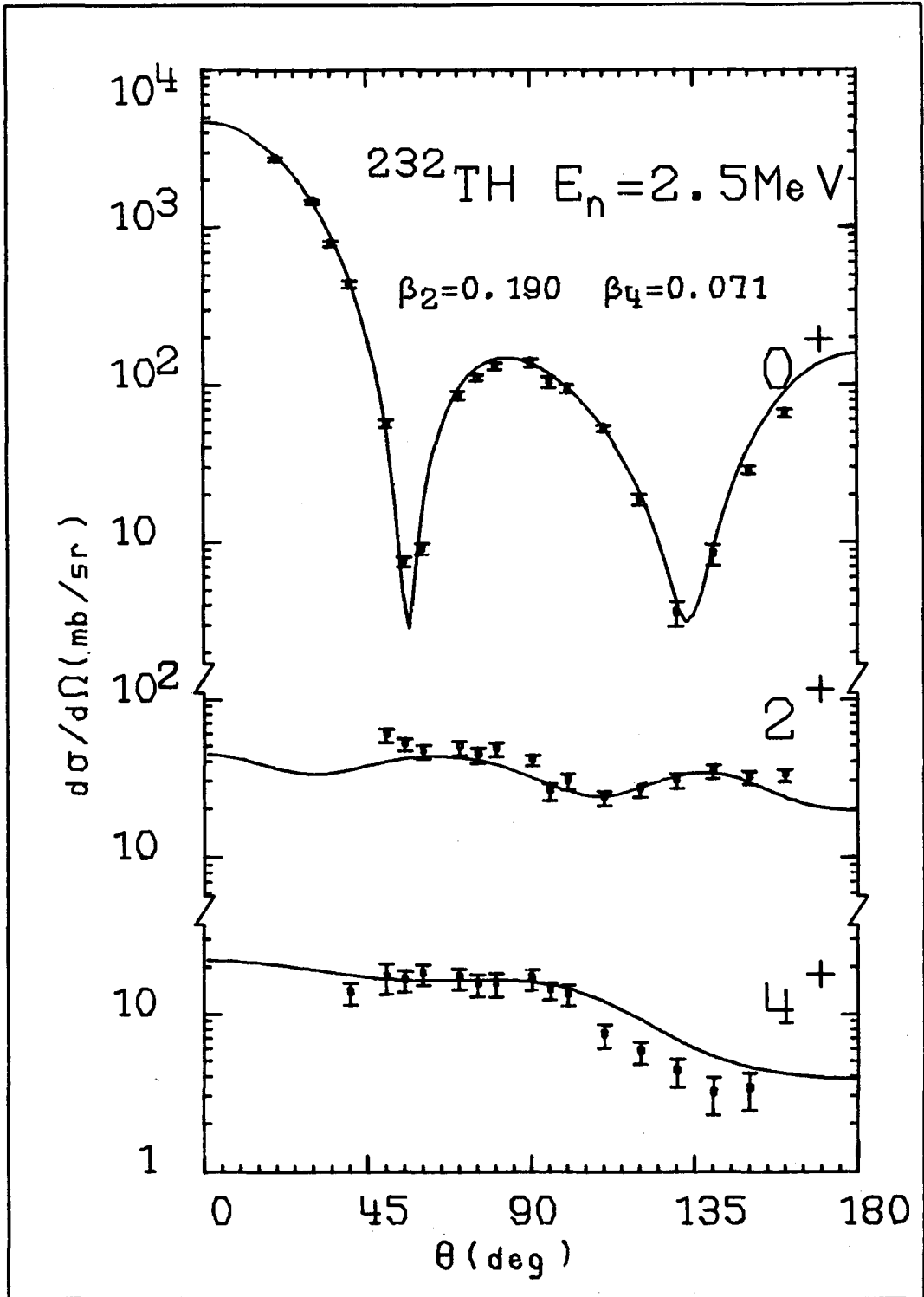


FIGURE 7

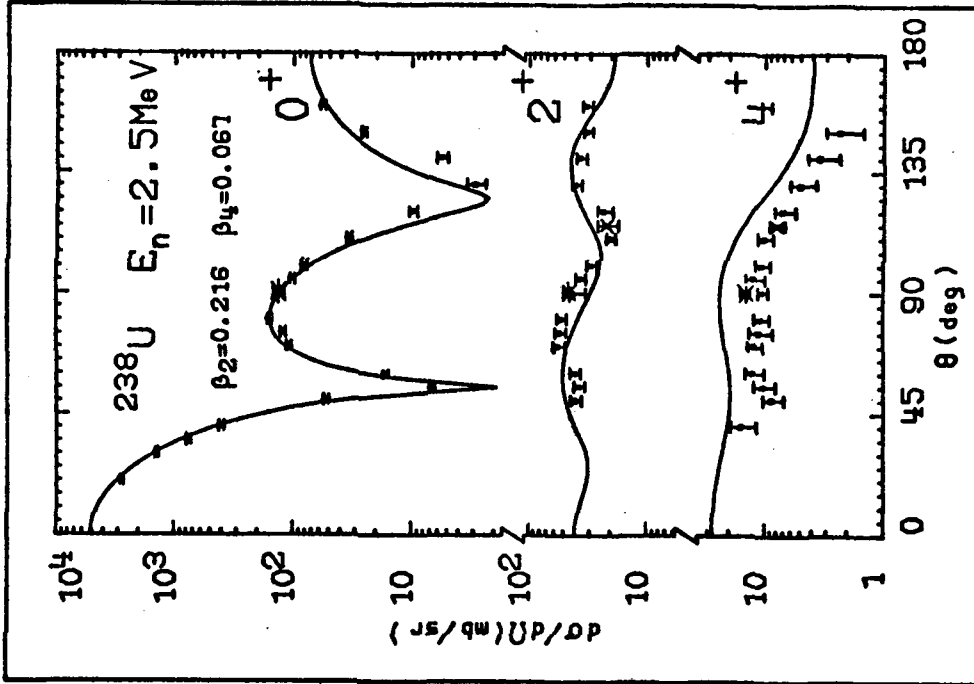


FIGURE 8a

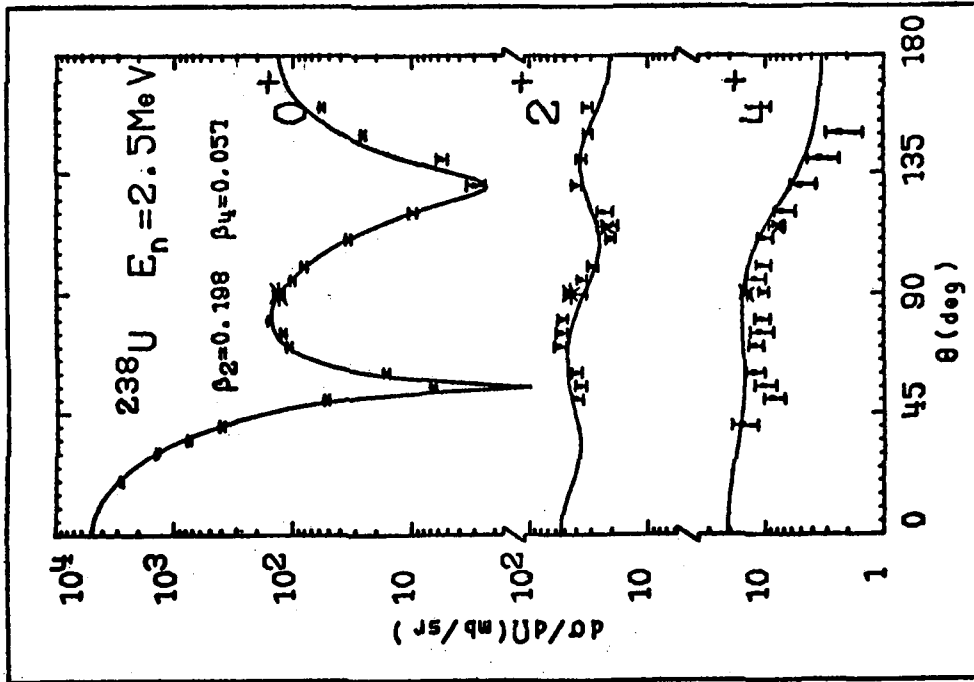


FIGURE 8b

000874